Ultrafast Laser-Shock-Induced Confined Metaphase Transformation for Direct Writing of Black Phosphorus Thin Films

Gang Qiu, Qiong Nian, Maithilee Motlag, Shengyu Jin, Biwei Deng, Yexin Deng, Adam R. Charnas, Peide D. Ye, and Gary J. Cheng**

Few-layer black phosphorus (BP) has emerged as one of the most promising candidates for post-silicon electronic materials due to its outstanding electrical and optical properties. However, lack of large-scale BP thin films is still a major roadblock to further applications. The most widely used methods for obtaining BP thin films are mechanical exfoliation and liquid exfoliation. Herein, a method of directly synthesizing continuous BP thin films with the capability of patterning arbitrary shapes by employing ultrafast laser writing with confinement is reported. The physical mechanism of confined laser metaphase transformation is understood by molecular dynamics simulation. Ultrafast laser ablation of BP layer under confinement can induce transient nonequilibrium high-temperature and high-pressure conditions for a few picoseconds. Under optimized laser intensity, this process induces a metaphase transformation to form a crystalline BP thin film on the substrate. Raman spectroscopy, atomic force microscopy, and transmission electron microscopy techniques are utilized to characterize the morphology of the resulting BP thin films. Field-effect transistors are fabricated on the BP films to study their electrical properties. This unique approach offers a general methodology to mass produce large-scale patterned BP films with a one-step manufacturing process that has the potential to be applied to other 2D materials.

Since the rise of graphene,[1,2] we have witnessed a "gold rush" in 2D material research. The atomic layered nature of 2D materials is considered a promising avenue as silicon technology encounters its bottleneck with further scaling. Tremendous efforts have been made to unveil the properties and potential applications of a large catalog of 2D layered materials including graphene,[1,3,4] black phosphorus,[5–7] transition metal dichalcogenides (TMDs),[8] etc. Black phosphorus (BP), the monolayer form of which is known as phosphorene, is one of the most intriguing candidates among all the 2D materials and has been intensely studied since it was first isolated in 2014.[5,6] A BP 2D crystal layer has an atomic puckered honeycomb structure which is similar to graphene. Bulk BP is an intrinsic p-type semiconductor, with slight ambipolar behavior due to its narrow bandgap nature. It has outstanding electrical properties such as high hole mobility,[5–7,9] large on/off ratio,[5–7,9] and a tunable bandgap.[10–13] Furthermore, by proper device engineering, such as adopting low work-function metal contact,[14] ALD doping,[15] and gate electrostatic doping,[16] n-type transistors with high electron mobility are also realized. Thereby, it has great potential to be used as ultrathin transistor channel material and further push CMOS scaling trend. In addition to extraordinary electrical properties, the ultrathin 2D BP also has superior mechanical flexibility and durability,[10,17] thus showing promise as a possible flexible electronics component.

Despite the promising qualities of BP, the lack of large-scale films remains a major obstacle against further BP research and

G. Qiu, Dr. Y. Deng, A. R. Charnas, Prof. P. D. Ye
School of Electrical and Computer Engineering
Purdue University
West Lafayette, IN 47907, USA
E-mail: yep@purdue.edu
G. Qiu, M. Motlag, S. Jin, B. Deng, Dr. Y. Deng, A. R. Charnas, Prof. P. D. Ye, Prof. G. J. Cheng
Birck Nanotechnology West Lafayette
Purdue University
West Lafayette, IN 47907, USA
E-mail: gjcheng@purdue.edu

DOI: 10.1002/adma.201704405

Prof. Q. Nian
Department of Mechanical Engineering
Arizona State University
Tempe, AZ 85281, USA
M. Motlag, S. Jin, B. Deng, Prof. G. J. Cheng
School of Industrial Engineering
Purdue University
West Lafayette, IN 47907, USA
Prof. G. J. Cheng
Institute of Technological Sciences
Wuhan University
Wuhan 430072, China

application studies. Just over a century ago, Bridgman first discovered bulk BP by applying high hydrostatic pressure (1.2 GPa) and high temperature (200 °C) to white phosphorus[18] in 1914. The shortcoming of this method is that it requires ultrahigh pressure and the starting material white phosphorus is highly volatile. Later other routes were proposed to prepare bulk BP such as using mercury as catalyst[19] and recrystallization from bismuth flux.[20–22] In 2008, Nilges et al.[23] proposed a fast low-pressure chemical vapor transport (CVT) method using AuSn as transport agent to produce bulk BP single crystals, which later was further simplified by Köpf et al.[24] As graphene ignited the 2D material research field, several top-down methods were established including mechanical[1,2,25] and liquid exfoliation method[26–31] to obtain sufficient amount of 2D thin films for research purposes. Shortly after these methods were applied to BP,[5,6,32–36] researchers were able to explore the atomic layer structure of BP comprehensively as a 2D material and demonstrate its potential electrical and optical applications. These exfoliation methods have caught eyes due to the availability of a single layer of material and compatibility with conventional CMOS fabrication processes. However, these methods also have their limitations. Liquid exfoliation is a candidate mass-production tool, however it tends to only yield small flake sizes varying from dozens to hundreds of nanometers, which constrains its potential for use in transistor device fabrication. Mechanical exfoliation with scotch tape is able to produce larger 2D films on the scale of a few micrometers, but the method itself is lacking in production efficiency and repeatability. Chemical vapor deposition has proved to be an effective method for growing wafer-scale monolayer 2D materials including graphene,[37,38] TMDs,[39] and boron nitride,[40] but so far it has not been achieved on BP because of its low melting temperature and strong chemical reactivity. Several processes with assistance of laser have been explored to produce BP thin films as well. For instance, pulsed laser deposition[41] method has been used to deposit few nanometers of amorphous BP thin films. Continuous-wave laser thinning has also been demonstrated to effectively produce thin films of 2D materials such as BP[42] and MoS_2.[43] Other methods include high-pressure transformation from red phosphorus thin films,[44] using scanning probe nanopatterning[45] and sonochemical synthesis method.[46]

In this study, we explore an innovative laser writing process—confined ultrafast pulsed laser deposition (CUPLD). We utilize ultrafast picosecond laser pulses to ablate continuous BP thin films from high-quality large bulk BP crystal. By adopting a confined ultrafast laser setup, the laser pulse is able to generate local high-temperature and high-pressure conditions, which triggers the metaphase transformation from ablated phosphorus to reconstructed BP thin films. The morphology and crystallinity of the BP films are characterized by techniques including atomic force microscopy (AFM), scanning electron microscopy (SEM), and transmission electron microscopy (TEM). Molecular dynamics simulations help to elucidate the physical mechanism of the ultrafast laser induced metaphase transformation process. This novel laser direct writing method not only introduces a fast route to produce large-scale BP thin films but also provides a one-step patterning process that potentially can be applied to other 2D materials.

Bulk black phosphorus crystals used for experiments were synthesized following the previously mentioned vapor transport method[24] (see the Experimental Section). The schematic process flow of manufacturing approach is illustrated in **Figure 1**. A large chunk of bulk BP (6 mm × 6 mm) with flat surface was chosen from synthesized bulk BP and placed on top of a quartz plate. A transparent substrate (e.g., sapphire, quartz, PET, etc.) was then mounted on top of bulk BP. The purpose of this transparent substrate is twofold: it provides a physical confinement to generate local high pressure and temperature while letting laser passing through; in the meantime, it serves as an in situ substrate where the BP thin films can be deposited. To ensure the substrate is in good contact with BP, the quartz plate and the substrate were tightly clamped together with bulk BP sandwiched in the middle. The experiment is carried out in a sealed chamber filled with argon to prevent photon-assisted oxidation effects[47] during laser ablation. Ultrafast laser pulses (wavelength: 1064 nm, pulse width: 5 ps) were generated by Fianium HE-1060 fiber laser source with the waveforms digitally controlled by computer. A scan algorithm was generated through the computer to adjust the angle of two reflecting mirrors so that the laser path can be manipulated and laser spot can be moved around the substrate. Upon exposure to the laser, the surface of the bulk BP absorbs the photon energy and then converts it into phonon energy through photon–phonon interaction which causes strong lattice vibrations that are vigorous enough to break P—P bonds and ablate BP from the bulk crystal. The benefit of the ultrafast laser pulses is to localize the laser energy to produce an almost instant high-pressure and high-temperature nonequilibrium condition before the energy dissipates away through lattice vibrations. This allows P—P bonds to reform into BP through a metaphase transformation process. The necessity of employing ultrafast picosecond laser pulse will be further investigated in the latter part of this paper.

One of the most preeminent advantages of this confined ultrafast laser direct writing method is that by designing the trace of the laser spot we can quickly pattern the 2D films into arbitrary shapes. In the meantime, it facilitates the manufacturing procedure by integrating patterning, ablation, and deposition into a one-step digitally controlled process. **Figure 2**a shows a direct written BP thin film patterned into the shape of the Purdue logo to demonstrate the potential of patterning arbitrary shapes of thin films with this technique. The film is verified to be conductive and continuous as shown in Figure 2b, indicating that the semiconducting crystalline nature of the BP is preserved. This confined laser writing method in principle can also be applied to other 2D materials. For example, we adapted the same method to write large-area graphene thin films (Figure 2c) ablated from highly oriented pyrolytic graphite (HOPG). Figure 2d shows the SEM image of various graphene thin films patterned using our method.

In order to examine the topography and quality of BP thin films, we performed Raman spectroscopy, TEM, and AFM experiments. **Figure 3**a shows the Raman spectrum of as-deposited BP films excited by a 532 nm laser. The A_g^1, B_{2g}, and A_g^2 Raman modes are located at 362, 440, and 468 cm^{-1}, respectively. The positions of characteristic Raman peaks match well with those of the bulk sample, indicating that the laser writing process preserved the orthorhombic crystalline structure of

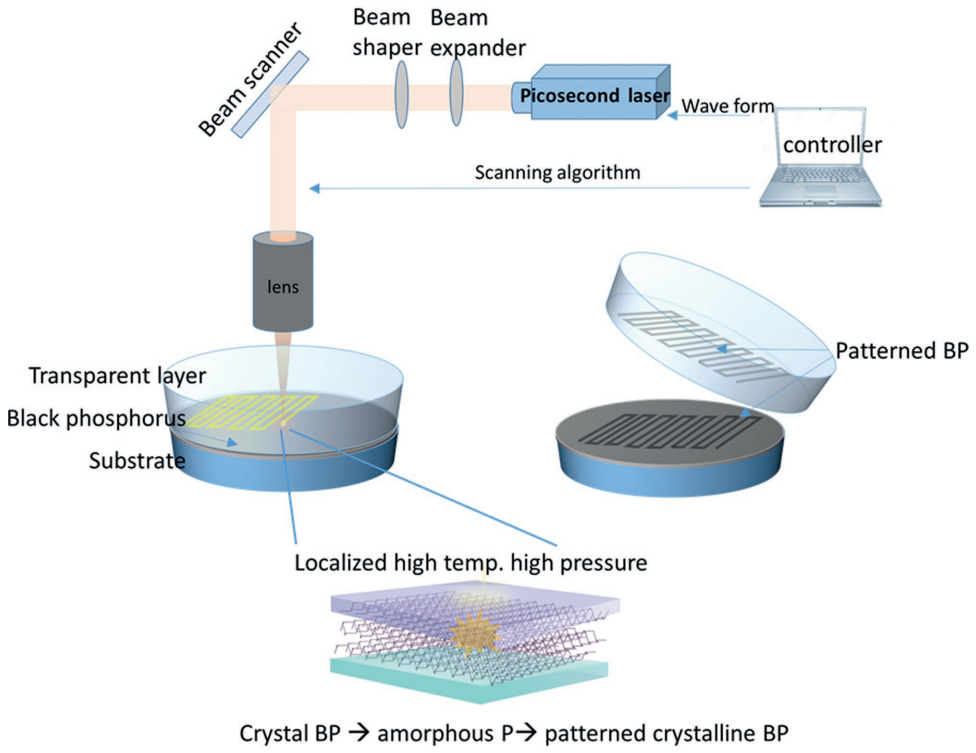

Figure 1. Experiment setup of fabrication of large-scale BP thin films by ultrafast laser direct writing.

BP. BP thin films were transferred onto a copper grid for TEM examination, and a representative resulting image is shown in Figure 3b. The periodic pattern (left inset) confirms the high degree of crystallinity of our CUPLD BP films. The spacing between primary neighboring patterns is 2.6 Å, corresponding to a (111) surface. The AFM image in Figure 3c reveals the surface morphology of the BP thin film. The film consists of many quadrangular shaped units with lateral size of nearly 1 µm. We systematically studied the thickness distribution of around 100 flakes, which is presented in a histogram in the Supporting Information. The average flake thickness is 38 nm and thinnest flake we found is 6.1 nm. The typical thickness ranges from around 10 to 100 nm. These small BP units stack on top of each other and pile up into a polycrystalline mesh. The reason why these units have similar shapes and sizes is not fully understood so far. We presume that as a strongly anisotropic material, the forming energy of P—P covalence bonds in certain directions is lower than the others and thus the BP films tend to reform into certain shapes. Similar shape of BP flakes was also reported by Seo et al.[48] using liquid exfoliation method where the sharp edge was assigned to (010) facet since it is an energetically more favorable orientation.

We further fabricated field-effect transistors (FETs) to explore the electrical properties of our CUPLD BP thin films. **Figure 4**a demonstrates the device structure schematically. The device was fabricated on indium tin oxide (ITO) glass as back gate with 20 nm ALD Al_2O_3 as a gate dielectric. More details of device fabrication can be found in the Experimental Section. The transfer curve and output curve of a 500 nm channel length FET device is shown as in Figure 4b,c. The device shows p-MOSFET behavior with on/off ratio on the order of 10. The back gate modulation is relatively small compared to few layer or monolayer BP FETs. The bandgap of BP can be strongly modulated from 0.3 to over 1.5 eV[5,49,50] by reducing the thickness from bulk to monolayer. The AFM image (Figure 3c) confirms that the BP film consists of small units with a thickness from tens to a hundred nanometers, so the band structure of the BP thin film should be closer to the bulk form with small bandgap. The flake thickness is generally larger than the maximum depletion width, meaning that the gate loses control over the top channel region of the thick flake and the device cannot be effectively turned off. Therefore, it is reasonable for the FET device to exhibit a small on/off ratio. For fair comparison, we fabricated FET devices on mechanically exfoliated BP flakes with thickness similar to our CUPLD deposited BP films, which is typically 30–100 nm. The electrical performance of the mechanically exfoliated devices (shown in Figure S1, Supporting Information) was close to that of the CUPLD devices. This validates that the inferior on/off ratio is not due to the crystal quality of the film but simply because of the nature of narrow bandgap semiconductors.

The energy density of the laser pulse is a crucial factor to achieve high-quality BP thin films. At low laser energy (≈15 GW cm^{-2}), the photon energy is too low to break the interlayer van der Waals bond, and BP films cannot be ablated from the bulk. By increasing laser energy to ≈20 GW cm^{-2}, the photon energy reaches the threshold to break the P—P covalent bond and laser ablation occurs, so we can obtain BP films with reasonable quality and high coverage. However, if we keep increasing the laser energy, the lattice vibrations will be

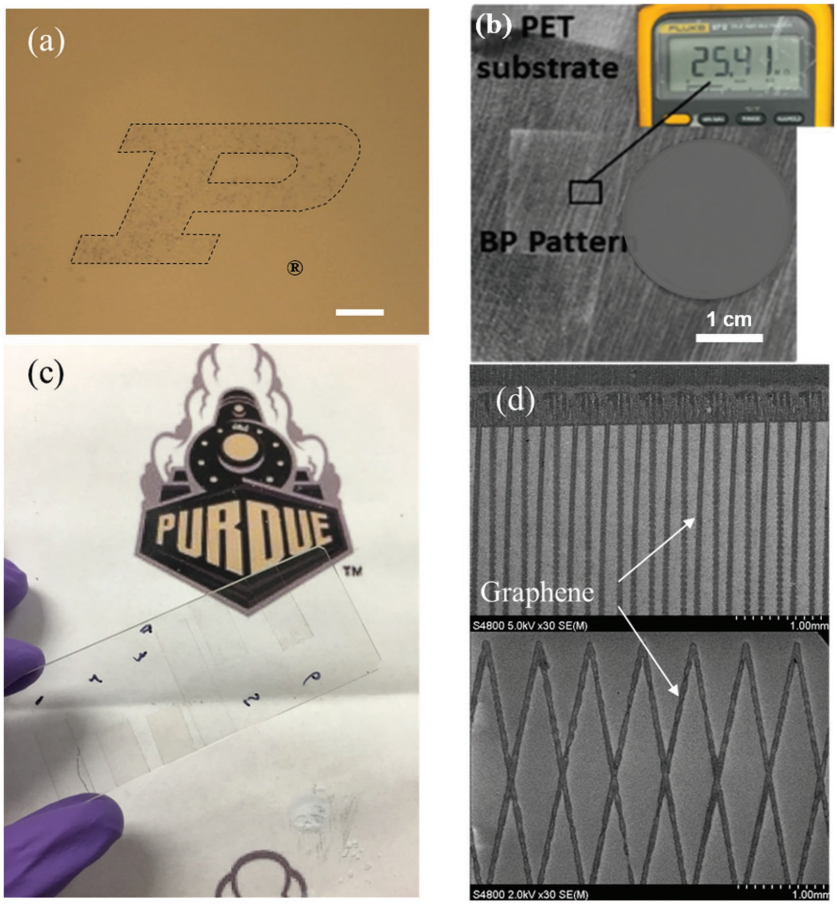

Figure 2. Demonstration of laser direct-writing method. a) An optical image of a BP thin film patterned into the shape of the Purdue logo. The scale bar is 10 um. The dotted line is a guide to the eye to show the contour of the BP film. b) An image of patterned BP films on PET substrate. The inset: the multimeter reading indicating the film is continuous and conductive. c) Large-area laser direct writing of graphene films ablated from HOPG. d) SEM images of graphene thin films with various patterns.

too vigorous and P—P covalent bonds will reorganize into red phosphorus. Therefore, the window for applicable laser energy density is in fact very narrow. This conclusion is confirmed by Raman spectra of BP thin films obtained with different laser powers, as shown in **Figure 5**a: the sample exposed to a laser with 15 GW cm^{-2} energy density does not show any BP Raman signals indicating no BP film is ablated; the one with 20 GW cm^{-2} energy density shows typical BP Raman signal with sharp peaks; as the energy increased to 30 GW cm^{-2}, the corresponding Raman spectrum indicates that red phosphorus is formed.

Molecular dynamics (MD) simulations give us a more insightful view of the microscopic mechanism of laser ablation. MD simulations were performed using LAMMPS to simulate laser ablation by adding different laser energy to the system at uniform intervals of 5 fs for a microcanonical ensemble (NVE simulation). More details about the simulation environment can be found in the Experimental Section. We found that ultrafast laser pulse can generate an instant high-pressure and high-temperature nonequilibrium condition. The maximum temperature and maximum pressure increase almost linearly as we increase the laser power (see **Figure 6**c,d). However, the metaphase transition of BP only happens in a very narrow laser energy window. Here to be consistent with our experiment, we choose three typical laser energy: 15, 20, and 30 GW cm^{-2} laser to provide a detailed physical picture of atomic structure change under each of the laser energy. At a lower laser energy of 15 GW cm^{-2}, ablation was not observed. As seen from Figure 5b, van der Waal forces between the black phosphorus layers weakened and the layers were observed to oscillate, however, the laser energy was not strong enough to ablate the BP layers. An interesting phenomenon was observed when the laser energy was increased to 20 GW cm^{-2}. The dangling P atoms reordered at high-pressure and temperature conditions under confinement (see Video S1, Supporting Information). This process was ultrafast and occurred within 10 ps. After the heat flux was removed from the system, nonequilibrium phase change of the system was observed and amorphous phosphorus was converted back to stable black phosphorus because of the local high-pressure and high-temperature conditions. This can be seen in Figure 5c. Because of the high kinetic energy, the phosphorus atoms sought their equilibrium positions and formed stable bonds at 20 GW cm^{-2}. A successful metaphase transition was observed at a laser intensity of 20 GW cm^{-2} where phosphorus atoms were reordered to black phosphorus due to the high-temperature and pressure conditions (see Video S2, Supporting Information). At 30 GW cm^{-2}, the energy of the system was very high and the atoms oscillated dramatically which created an obstacle in re-bonding of the system. As seen from Figure 5d, ablated P atoms fail to order themselves into BP atoms and chemical bonds cannot be formed at higher laser power (see Video S3, Supporting Information). High pressure in the range of 20–25 GPa and a high temperature of about 1200 K aided the structural phase transition in black phosphorus at 20 GW cm^{-2} as can be observed from Figure 6a,b.

The laser pulse width is also important in order to reach the desired nonequilibrium conditions for metaphase transition of black phosphorus. We adopted the picosecond ultrafast laser source because its pulse time is comparable to the critical time of the lattice vibration period, which is normally also within several picoseconds. After the short laser pulse the heat flux is removed and the energy can then be dissipated through phonon scattering. In this scenario, the metaphase transition is dominated by the transient nonequilibrium high-pressure and high-temperature condition. On the other hand, if a much longer laser pulse, for example, several nanoseconds, is applied, the local thermal energy will pile up before being dissipated through lattice vibrations and the transient nonequilibrium conditions will eventually be altered by the additional

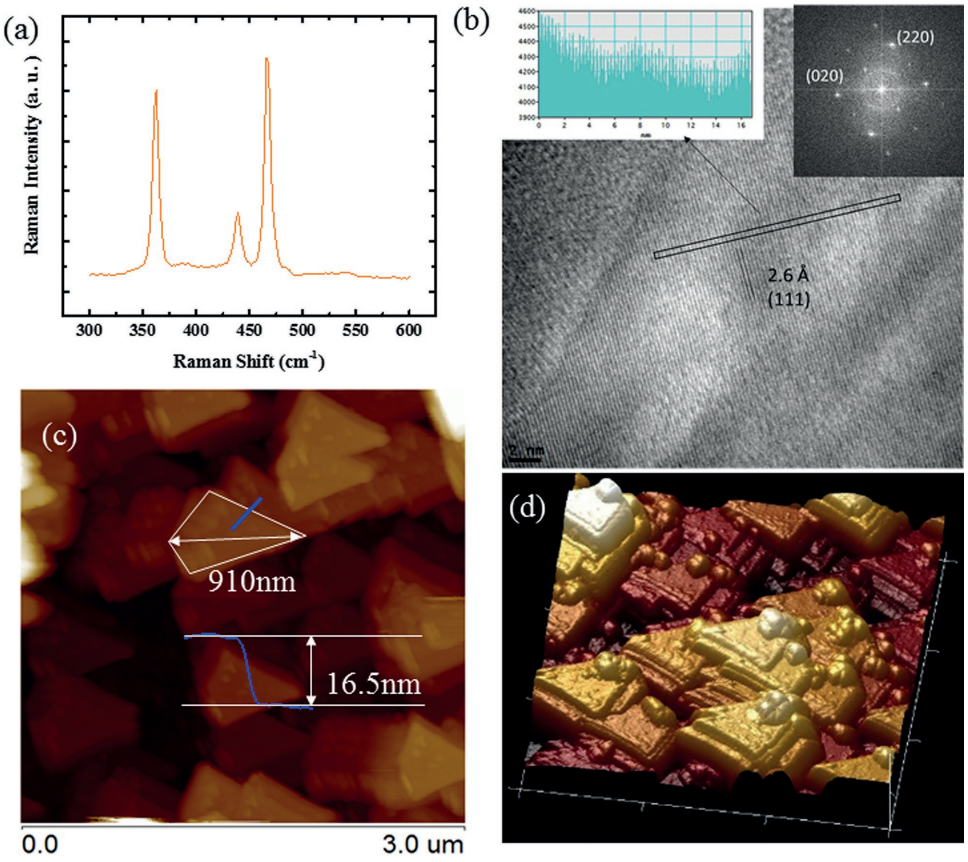

Figure 3. Characterization of BP thin film. a) Raman spectroscopy of BP thin film; b) TEM image of the BP film. The left inset shows the intersection profile within the black box. The right inset is the fast Fourier transform of the TEM image. c) AFM image showing the surface morphology of the BP film. d) 3D image of height profile.

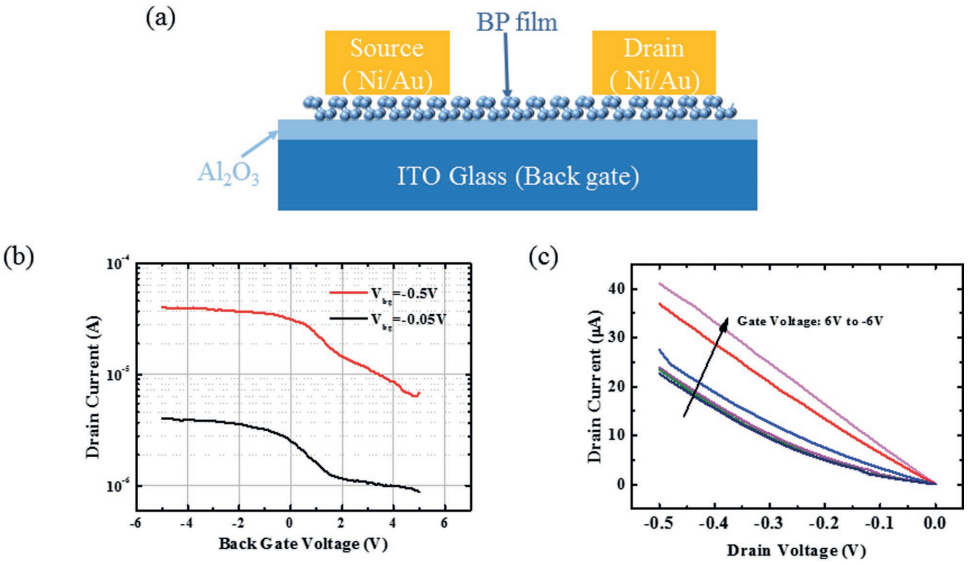

Figure 4. Electrical properties of thin film BP FET. a) Schematic diagram of FET device structure. b) Transfer curve and c) output curve of BP thin film transistors. The channel length of the device is 500 nm and the channel width is 2 μm.

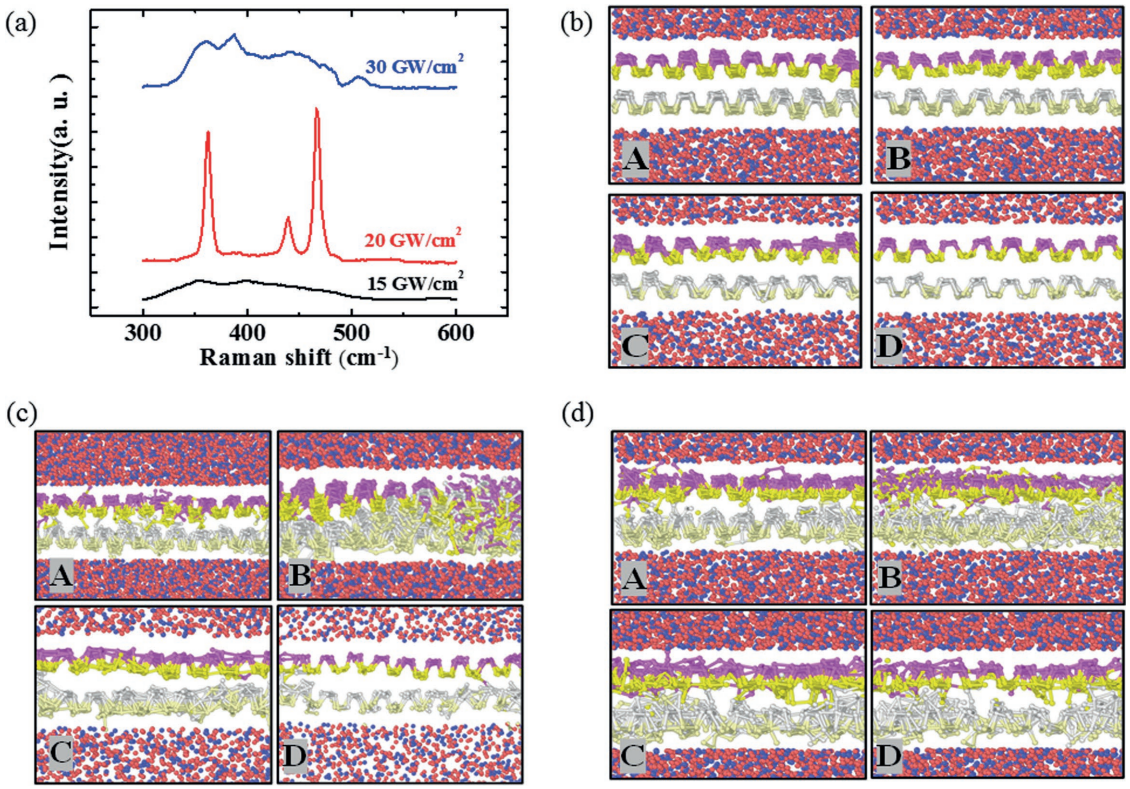

Figure 5. Impact of laser energy on BP thin films. a) Raman spectra of thin films obtained with different laser energy. b–d) The snapshots of BP films during laser ablation process with 15, 20, and 30 GW cm^{-2} in MD simulations. b) No ablation was observed at 15 GW cm^{-2}; P atoms are dislocated and reformed into BP through metaphase transformation at 20 GW cm^{-2}; P atoms are not able to reform into BP due to higher kinetic energy at 30 GW cm^{-2}.

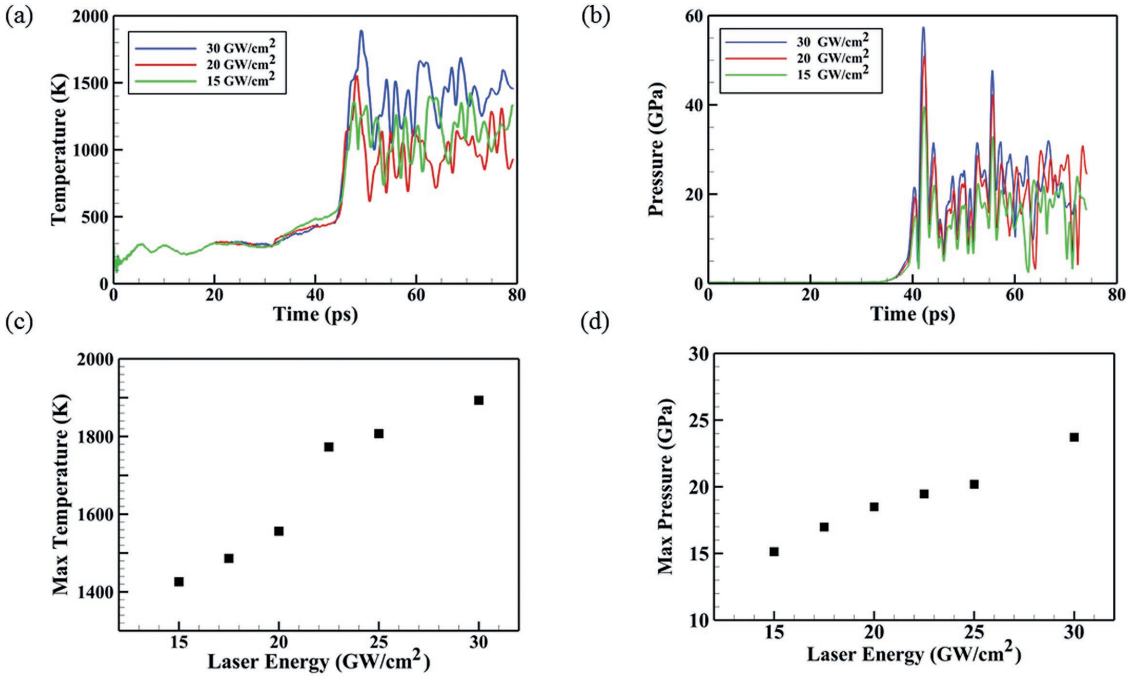

Figure 6. a) Temperature and b) pressure curves for equilibration (0–35 ps), laser heating (35–45 ps), and re-bonding (45–75 ps) molecular dynamic processes. c) Maximum temperature and d) maximum pressure extracted under different laser power.

thermal energy and the metaphase transition will not happen anymore. We have experimentally verified that after exposing to a nanosecond laser pulse, black phosphorus is converted into amorphous phosphorus (SEM image and Raman results can be found in the Supporting Information), which is also consistent with our MD simulation interpretation.

In conclusion, we presented an innovative approach, namely, CUPLD, to produce large-scale black phosphorus thin films by generating local high-temperature and high-pressure conditions through confinement. We demonstrated the feasibility of patterning large-scale arbitrary BP thin films as well as other 2D materials with this method. Raman spectroscopy, TEM, and AFM techniques were used to characterize the quality and morphology of BP thin films. FET devices were fabricated on the BP film with reasonable electrical properties. Molecular dynamics simulations were performed to study the physical mechanism of the laser-assisted metaphase transformation process. This approach represents a promising method to obtain BP thin films, not only because laser is a more maneuverable tool than mechanical or liquid exfoliation but also because potentially it can be adopted to pattern the films of other 2D materials. Meanwhile, the process is an intriguing and fast route for massive nanomanufacturing since it integrates ablation, deposition, and patterning into a one-step process.

Experimental Section

Bulk BP Crystal Growth: Precursor materials, consisting of 150 mg red phosphorus (Sigma-Aldrich, Powder, ≥99.99%), 8 mg tin (IV) iodide (powder), and 21 mg elemental tin (Sigma-Aldrich, Powder, ≥99%) were loaded into clean quartz ampoules with an inner diameter of 6 mm. Ampoules were evacuated to a vacuum strength of <0.01 mTorr and then sealed using a propane-oxygen torch, enclosing the precursor materials in a vacuum pocket roughly 10 cm long. Ampoules were then placed into a multizone furnace capable of maintaining a sufficient heat gradient across the sample volume. Over the course of the reaction, the side of the ampoule initially containing the precursor materials maintained a 50 °C temperature elevation over the empty side of the ampoule. The hot end containing the precursors was first heated to 750 °C from room temperature over the course of 3 h, then held at that temperature for 1 h. The hot end was then cooled over 3 h to 500 °C, held there for three additional hours, then cooled to 100 °C slowly over the next 10 h. This process typically yields large (centimeter scale) high-purity single-crystal flakes radiating from a central nucleation point on the cold end of the ampoule.

FET Device Fabrication: Special transparent substrates were prepared for CUPLD in for compatibility with FET fabrication. 20 nm Al_2O_3 was deposited on ITO glass at 200 °C: Al_2O_3 serves as dielectric layer; ITO can be used as the back gate and in the meantime as a conductive layer that facilitates electron beam lithography in the subsequent step. After CUPLD, source and drain regions were patterned by electron beam lithography and Ni/Au metal contacts were deposited by electron beam evaporator. The channel length of the devices is 500 nm and the channel width is 2 μm.

Molecular Dynamics Simulation: Two single black phosphorus layers of dimension 100 Å × 100 Å were modeled between amorphous silica using VESTA. Periodic boundary conditions were imposed along *X* and *Y* directions and fixed boundary condition was imposed along the *Z* direction. System equilibration was carried out at 300 K with Nosé–Hoover thermostat. The Stillinger–Weber (SW) potential was developed by using ab initio valence force field method by Jiang et al. Parametrization of Stillinger–Weber potential based on valence force field model was implemented in these simulations to define P—P bonds and Lennard Jones potential was used to define interlayer interactions. The interactions between silica and black phosphorus were neglected since the focus of this work was to observe the influence of laser heating on black phosphorus. Silica was modeled to ensure that the high stresses developed in black phosphorus layers during laser heating were maintained. A timestep of 0.1 ps was used to integrate the equations of motion. Heat flux was added to multilayer black phosphorus with an NVE ensemble to simulate laser heating. To simulate dynamic bond creation and breaking, Stillinger–Weber potential was turned off and a harmonic bond potential was defined. The results were visualized using the OVITO package. To further validate the metaphase transformation of amorphous to crystalline black phosphorus, radial distribution function was investigated for structural characterization.

Supporting Information

Supporting Information is available from the Wiley Online Library or from the author.

Acknowledgements

G.Q., Q.N. and M.M. contributed equally to this work. G.J.C. acknowledges financial support from U.S. National Science Foundation and National Research Council Senior Research Fellowship program. P.D.Y. acknowledges the support from U.S. National Science Foundation and Department of Defense.

Conflict of Interest

The authors declare no conflict of interest.

Keywords

black phosphorus, direct writing, thin films

Received: August 4, 2017
Revised: September 29, 2017
Published online:

[1] K. S. Novoselov, A. K. Geim, S. V. Morozov, D. Jiang, M. I. Katsnelson, I. V. Grigorieva, S. V. Dubonos, A. A. Firsov, *Nature* **2005**, *438*, 197.
[2] K. S. Novoselov, A. K. Geim, S. V. Morozov, D. Jiang, Y. Zhang, S. V. Dubonos, I. V. Grigorieva, A. A. Firsov, *Science* **2004**, *306*, 666.
[3] Y. B. Zhang, Y. W. Tan, H. L. Stormer, P. Kim, *Nature* **2005**, *438*, 201.
[4] A. H. Castro Neto, F. Guinea, N. M. R. Peres, K. S. Novoselov, A. K. Geim, *Rev. Mod. Phys.* **2009**, *81*, 109.
[5] H. Liu, A. Neal, Z. Zhu, Z. Luo, X. Xu, *ACS Nano* **2014**, *8*, 4033.
[6] L. Li, Y. Yu, G. J. Ye, Q. Ge, X. Ou, H. Wu, D. Feng, X. H. Chen, Y. Zhang, *Nat. Nanotechnol.* **2014**, *9*, 372.
[7] F. Xia, H. Wang, Y. Jia, *Nat. Commun.* **2014**, *5*, 4458.
[8] B. Radisavljevic, A. Radenovic, J. Brivio, V. Giacometti, A. Kis, *Nat. Nanotechnol.* **2011**, *6*, 147.
[9] Y. Du, H. Liu, Y. Deng, P. D. Ye, *ACS Nano* **2014**, *8*, 10035.
[10] R. Fei, L. Yang, *Nano Lett.* **2014**, *14*, 2884.
[11] J. Kim, S. S. Baik, S. H. Ryu, Y. Sohn, S. Park, B.-G. Park, J. Denlinger, Y. Yi, H. J. Choi, K. S. Kim, *Science* **2015**, *349*, 723.
[12] B. Deng, V. Tran, Y. Xie, H. Jiang, C. Li, Q. Guo, X. Wang, H. Tian, S. J. Koester, H. Wang, J. J. Cha, Q. Xia, L. Yang, F. Xia, *Nat. Commun.* **2017**, *8*, 14474.

[13] B. Liu, M. Köpf, A. N. Abbas, X. Wang, Q. Guo, Y. Jia, F. Xia, R. Weihrich, F. Bachhuber, F. Pielnhofer, H. Wang, R. Dhall, S. B. Cronin, M. Ge, X. Fang, T. Nilges, C. Zhou, *Adv. Mater.* **2015**, *27*, 4423.
[14] D. J. Perello, S. H. Chae, S. Song, Y. H. Lee, *Nat. Commun.* **2015**, *6*, 7809.
[15] H. Liu, A. T. Neal, M. Si, Y. Du, P. D. Ye, *IEEE Electron Device Lett.* **2014**, *35*, 795.
[16] M. Buscema, D. J. Groenendijk, G. A. Steele, H. S. J. van der Zant, A. Castellanos-Gomez, *Nat. Commun.* **2014**, *5*, 1.
[17] Q. Wei, X. Peng, *Appl. Phys. Lett.* **2014**, *104*, 251915.
[18] P. W. Bridgman, *J. Am. Chem. Soc.* **1914**, *36*, 1344.
[19] E. I. Jahre, D. Phosphor, W. Gunther, D. P. Stofidrucken, H. Krebs, H. Weitz, K. Worms, *J. Inorg. Chem.* **1943**, *280*, 119.
[20] A. Brown, S. Rundqvist, *Acta Crystallogr.* **1965**, *19*, 684.
[21] Y. Maruyama, S. Suzuki, K. Kobayashi, S. Tanuma, *Phys. B+C* **1981**, *105*, 99.
[22] M. Baba, F. Izumida, Y. Takeda, A. Morita, *Jpn. J. Appl. Phys.* **1989**, *28*, 1019.
[23] T. Nilges, M. Kersting, T. Pfeifer, *J. Solid State Chem.* **2008**, *181*, 1707.
[24] M. Köpf, N. Eckstein, D. Pfister, C. Grotz, I. Krüger, M. Greiwe, T. Hansen, H. Kohlmann, T. Nilges, *J. Cryst. Growth* **2014**, *405*, 6.
[25] M. S. Dresselhaus, P. T. Araujo, *ACS Nano* **2010**, *4*, 6297.
[26] Y. Hernandez, V. Nicolosi, M. Lotya, F. Blighe, Z. Sun, S. De, I. T. McGovern, B. Holland, M. Byrne, Y. Gunko, J. Boland, P. Niraj, G. Duesberg, S. Krishnamurti, R. Goodhue, J. Hutchison, V. Scardaci, A. C. Ferrari, J. N. Coleman, *Nat. Nanotechnol.* **2008**, *3*, 563.
[27] J. N. Coleman, *Adv. Funct. Mater.* **2009**, *19*, 3680.
[28] X. Cui, C. Zhang, R. Hao, Y. Hou, *Nanoscale* **2011**, *3*, 2118.
[29] J. N. Coleman, *Acc. Chem. Res.* **2013**, *46*, 14.
[30] W. Du, X. Jiang, L. Zhu, *J. Mater. Chem. A* **2013**, *1*, 10592.
[31] A. Ciesielski, P. Samorì, *Chem. Soc. Rev.* **2014**, *43*, 381.
[32] S. P. Koenig, R. A. Doganov, H. Schmidt, A. H. Castro Neto, B. Özyilmaz, *Appl. Phys. Lett.* **2014**, *104*, 103106.
[33] D. Hanlon, C. Backes, E. Doherty, C. S. Cucinotta, N. C. Berner, C. Boland, K. Lee, A. Harvey, P. Lynch, Z. Gholamvand, S. Zhang, K. Wang, G. Moynihan, A. Pokle, Q. M. Ramasse, N. McEvoy, W. J. Blau, J. Wang, G. Abellan, F. Hauke, A. Hirsch, S. Sanvito, D. D. O'Regan, G. S. Duesberg, V. Nicolosi, J. N. Coleman, *Nat. Commun.* **2015**, *6*, 8563.
[34] V. Sresht, A. a. H. Pádua, D. Blankschtein, *ACS Nano* **2015**, *9*, 8255.
[35] P. Yasaei, B. Kumar, T. Foroozan, C. Wang, M. Asadi, D. Tuschel, J. E. Indacochea, R. F. Klie, A. Salehi-khojin, *Adv. Mater.* **2015**, *27*, 1.
[36] H. Zhou, Y. Du, P. D. Ye, *Appl. Phys. Lett.* **2016**, *108*, 202102.
[37] K. V Emtsev, A. Bostwick, K. Horn, J. Jobst, G. L. Kellogg, L. Ley, J. L. McChesney, T. Ohta, S. A. Reshanov, J. Röhrl, E. Rotenberg, A. K. Schmid, D. Waldmann, H. B. Weber, T. Seyller, *Nat. Mater.* **2009**, *8*, 203.
[38] A. N. Obraztsov, *Nat. Nanotechnol.* **2009**, *4*, 212.
[39] H. Wang, L. Yu, Y.-H. Lee, W. Fang, A. Hsu, P. Herring, M. Chin, M. Dubey, L.-J. Li, J. Kong, T. Palacios, *2012 Int. Electron Devices Meeting* **2012**, *1*, 4.6.1.
[40] Y. Shi, C. Hamsen, X. Jia, K. K. Kim, A. Reina, M. Hofmann, A. L. Hsu, K. Zhang, H. Li, Z. Y. Juang, M. S. Dresselhaus, L. J. Li, J. Kong, *Nano Lett.* **2010**, *10*, 4134.
[41] Z. Yang, J. Hao, S. Yuan, S. Lin, H. M. Yau, J. Dai, S. P. Lau, *Adv. Mater.* **2015**, *27*, 3748.
[42] M. J. L. F. Rodrigues, C. J. S. de Matos, Y. W. Ho, H. Peixoto, R. E. P. de Oliveira, H. Y. Wu, A. H. C. Neto, J. Viana-Gomes, *Adv. Mater.* **2016**, *28*, 10693.
[43] A. Castellanos-Gomez, M. Barkelid, A. M. Goossens, V. E. Calado, H. S. J. Van Der Zant, G. a. Steele, *Nano Lett.* **2012**, *12*, 3187.
[44] X. Li, B. Deng, X. Wang, S. Chen, M. Vaisman, S. Karato, G. Pan, M. L. Lee, J. Cha, H. Wang, F. Xia, *2D Mater.* **2015**, *2*, 031002.
[45] X. Liu, K. S. Chen, S. A. Wells, I. Balla, J. Zhu, J. D. Wood, M. C. Hersam, *Adv. Mater.* **2017**, *29*, 1604121.
[46] S. H. Aldave, M. N. Yogeesh, W. Zhu, J. Kim, S. S. Sonde, A. P. Nayak, D. Akinwande, *2D Mater.* **2016**, *3*, 014007.
[47] A. Favron, E. Gaufrès, F. Fossard, A.-L. Phaneuf-L'Heureux, N. Y.-W. Tang, P. L. Lévesque, A. Loiseau, R. Leonelli, S. Francoeur, R. Martel, *Nat. Mater.* **2015**, *14*, 826.
[48] S. Seo, H. U. Lee, S. C. Lee, Y. Kim, H. Kim, J. Bang, J. Won, Y. Kim, B. Park, J. Lee, *Sci. Rep.* **2016**, *6*, 23736.
[49] S. Zhang, J. Yang, R. Xu, F. Wang, W. Li, M. Ghufran, Y. W. Zhang, Z. Yu, G. Zhang, Q. Qin, Y. Lu, *ACS Nano* **2014**, *8*, 9590.
[50] M. Buscema, D. J. Groenendijk, S. I. Blanter, G. A. Steele, H. S. J. van der Zant, A. Castellanos-Gomez, *Nano Lett.* **2014**, *14*, 3347.

